PHOTONICS Research

Experimental witnessing for entangled states with limited local measurements

Gaoyan Zhu,[1] Chengjie Zhang,[2,3] Kunkun Wang,[1] Lei Xiao,[1] and Peng Xue[1,*]

[1]Beijing Computational Science Research Center, Beijing 100084, China
[2]School of Physical Science and Technology, Ningbo University, Ningbo 315211, China
[3]State Key Laboratory of Precision Spectroscopy, School of Physics and Electronic Science, East China Normal University, Shanghai 200241, China
*Corresponding author: gnep.eux@gmail.com

Received 3 May 2022; revised 28 June 2022; accepted 28 June 2022; posted 30 June 2022 (Doc. ID 462212); published 15 August 2022

We experimentally demonstrate a method for detection of entanglement via construction of entanglement witnesses from a limited fixed set of local measurements ($\mathcal{M}$). Such a method does not require *a priori* knowledge about the form of the entanglement witnesses. It is suitable for a scenario where a full state tomography is not available, but the only resource is a limited set of $\mathcal{M}$. We demonstrate the method on pure two-qubit entangled states and mixed two-qubit entangled states, which emerge from photonic implementation of controllable quantum noisy channels. The states we select are motivated by realistic experimental conditions, and we confirm it works well for both cases. Furthermore, possible generalizations to higher-dimensional bipartite systems have been considered, which can potentially detect both decomposable and indecomposable entanglement witnesses. Our experimental results show perfect validity of the method, which indicates that even a limited set of local measurements can be used for quick entanglement detection and further provide a practical test bed for experiments with entanglement witnesses.

https://doi.org/10.1364/PRJ.462212

1. INTRODUCTION

Quantum entanglement, which lies at the heart of the foundations of quantum mechanics, is a crucial resource for quantum information science [1,2]. For a given state, how to determine whether it is entangled or not is a fundamental question in quantum entanglement theory. In the past two decades since the definition of entanglement was clarified in Ref. [3], tons of research have been reported related to this subject, such as the well-known positive partial transpose criterion [4], the computable cross norm criterion (or matrix realignment criterion) [5,6], the permutation separability criterion [7,8], and entanglement witnesses [9–17]. Entanglement witnesses accomplish this task without requiring full state tomography. Thus, several types of entanglement witnesses have been defined and studied theoretically [18–32] and have been demonstrated in various physical systems [33–39].

Unlike the other criteria in which it is assumed that the state density matrix is preknown, entanglement witnesses are Hermitian operators and designed directly for detection of entanglement for states. Rather, an operator W that acts on a bipartite system is an entanglement witness if and only if $\mathrm{Tr}(\rho_s W) \geq 0$ for all separable states ρ_s and $\mathrm{Tr}(\rho_e W) < 0$ for, at least, one entangled state ρ_e. Entanglement witnesses completely characterize separable states and allow to detect entanglement experimentally [40]. Moreover, a witness W is optimal if for any $R \geq 0$ an operator $W - R$ is no longer a witness [41]. Optimal entanglement witnesses are the best entanglement detectors, that is, W is optimal if and only if there is no other witness that detects more quantum entangled states than W does. A witness, which is not optimal, may be optimized via a suitable optimization procedure [41]. It is, therefore, clear that knowing all optimal entanglement witnesses one is able to detect all entangled states. In a recent work, Riccardi *et al.* [42] proposed a method to construct entanglement witnesses from a limited fixed set of local measurements, which performed on two-qubit systems. This method fits within a scenario that a full state tomography is not available, whereas only a smaller resource as a measurements set $\mathcal{M}$ is available. Such a method completely characterizes the class of entanglement witnesses of the form $W = P^{\Gamma}$ where the superscript Γ denotes a partial transposition, that can be derived from $\mathcal{M}$. Designing a witness for an arbitrary entangled state, especially for mixed states is not easy since the problem of separability of mixed states appears to be extremely complex; whereas due to the decoherence phenomenon, in laboratories we unavoidably deal with mixed states rather than pure ones.

In this paper, we experimentally demonstrated the method in Ref. [42] for detecting entanglement of both pure and mixed two-qubit states. The mixed states we select are motivated by

realistic experimental conditions, which emerge from four typical single-qubit entanglement breaking channels, i.e., Pauli channels, dephasing channels, depolarizing channels, and amplitude damping channels. The features of requiring low measurement resources and no *a priori* knowledge about the witness forms show the widespread application and experimental feasibility of the method, thus, providing a practical test bed for quick entanglement detection. Furthermore, we experimentally explore the possible extensions to higher-dimensional bipartite systems, which can be used to detect decomposable and indecomposable entanglement witnesses.

2. THEORETICAL SCENARIOS

A two-qubit entanglement witness can be decomposed as

$$W = \sum_{i,j} T_{ij}\sigma_i \otimes \sigma_j, \tag{1}$$

with $\sigma_i \in \{\sigma_0, \sigma_1, \sigma_2, \sigma_3\}$, where σ_0 represents a two-dimensional identity matrix and σ_1, σ_2, and σ_3 are Pauli matrices. Given a limited set of measurements $\mathcal{M} = \{\sigma_1 \otimes \sigma_1, \sigma_2 \otimes \sigma_2, \sigma_3 \otimes \sigma_3\}$, witnesses of the below form can be constructed:

$$W = \alpha\sigma_0 \otimes \sigma_0 + \sum_{i=1,2,3} (a_i\sigma_0 \otimes \sigma_i + b_i\sigma_i \otimes \sigma_0) + \sum_{i=1,2,3} c_i\sigma_i \otimes \sigma_i, \tag{2}$$

where α, a_i, b_i, c_i are real parameters. We focus only on characterization of witnesses within the family of Eq. (2) that are of the form

$$W = P^{\Gamma}. \tag{3}$$

Therefore, P consists of only terms from the limited source $\mathcal{M}$.

It is proven in Ref. [42] that, there are six families of rank-1 projectors $|\psi\rangle\langle\psi|$ within the class of Eq. (2),

$$\begin{aligned} &|\varphi_1\rangle = a|\Phi^+\rangle + b|\Phi^-\rangle; |\varphi_2\rangle = a|\Psi^+\rangle + b|\Psi^-\rangle; \\ &|\varphi_3\rangle = a|\Phi^+\rangle + b|\Psi^+\rangle; |\varphi_4\rangle = a|\Phi^-\rangle + b|\Psi^-\rangle; \\ &|\varphi_5\rangle = a|\Phi^+\rangle + ib|\Psi^-\rangle; |\varphi_6\rangle = a|\Phi^-\rangle + ib|\Psi^+\rangle, \end{aligned} \tag{4}$$

where $|\Phi^{\pm}\rangle = (|00\rangle \pm |11\rangle)/\sqrt{2}$ and $|\Psi^{\pm}\rangle = (|01\rangle \pm |10\rangle)/\sqrt{2}$ are the Bell states; $a, b \in \mathbb{R}$ and satisfy $a^2 + b^2 = 1$.

In return, six families of entanglement witness that are of the form as Eq. (3) can be derived:

$$W_k = |\phi_k\rangle\langle\phi_k|^{\Gamma}, \tag{5}$$

where $k = 1, 2, \cdots, 6$. As an example, $W_1 = |\varphi_1\rangle\langle\varphi_1|$ decomposed as the form of Eq. (2) is given by

$$W_1 = \frac{1}{4}[\sigma_0 \otimes \sigma_0 + \sigma_3 \otimes \sigma_3 + (a^2 - b^2)\sigma_1 \otimes \sigma_1 + (a^2 - b^2)\sigma_2 \otimes \sigma_2 + 2ab(\sigma_3 \otimes \sigma_0 + \sigma_0 \otimes \sigma_3)], \tag{6}$$

which consists of only terms of measurement $\mathcal{M}$.

Then, for a given two-qubit state ρ, to identify whether it is entangled or not, we perform all the local measurements of $\mathcal{M}$ after which $\mathrm{Tr}(W_k\rho)$ is evaluated for each k. To find a value of $\mathrm{Tr}(W_k\rho)$ below zero, we minimize the value $\mathrm{Tr}(W_k\rho)$ over a and b for each k. If a negative value is obtained, then, the state is identified as entangled, and at the same time, a corresponding optimal witness for this state is defined. Such a postprocess implies that the method requires no *a priori* knowledge about the form of the entanglement witnesses.

3. EXPERIMENTAL DEMONSTRATION

In the experiment, we test the performance of the procedure with pure entangled two-qubit states of the form of Eq. (7) and multiple families of mixed entangled two-qubit states, which are generated by sending one party of the maximally entangled state $|\Phi^+\rangle$ through four types of single-qubit entanglement breaking channels, i.e., Pauli channels, dephasing channels, depolarizing channels, and amplitude damping channels, acting on one of the qubits. The experimental setup is illustrated in Fig. 1(a).

In our experiment, polarizations of the photon pairs are generated in a pure entangled state,

$$|\phi\rangle = \alpha|HH\rangle + \sqrt{1-\alpha^2}|VV\rangle, \tag{7}$$

by setting the angle of the half-wave plate (HWP) in front of the β-barium borate (BBO) to $0.5\arcsin\alpha$ with a fidelity higher than 97%. Here $|H\rangle = |0\rangle$ and $|V\rangle = |1\rangle$ represent the horizontal and vertical polarizations of photons, respectively. The fidelity is defined [43] as $F(\rho_{\mathrm{th}}, \rho_{\mathrm{exp}}) = (\mathrm{Tr}\sqrt{\sqrt{\rho_{\mathrm{th}}}\rho_{\mathrm{exp}}\sqrt{\rho_{\mathrm{th}}}})^2$, which can be evaluated from the reconstruction of the states via a full state tomography [44].

The mixed two-qubit entangled states emerge from four typical types of quantum noisy channels, i.e., Pauli channels, dephasing channels, depolarizing channels, and amplitude damping channels, acting on one of the qubits. These noisy channels are selected to show the validity of the method when applying it in a realistic experimental environment. The initial state is prepared in $(|HH\rangle + |VV\rangle)/\sqrt{2}$. Quantum noisy channels are completely positive trace-preserving maps $\mathcal{N}$ acting on a quantum state in a d-dimensional Hilbert space $\mathcal{H}^d$, which can be mathematically described as

$$\rho \mapsto \sum_i M_i\rho M_i^{\dagger}, \tag{8}$$

where M_i are the Kraus operators, satisfying $\sum_i M_i^{\dagger}\rho M_i = I$.

Taking a single-qubit Pauli channel as an example (see Appendix A for details on realizations of other noisy channels), the Kraus operators are given by $M_1 = \sqrt{p_0}\sigma_0$, $M_2 = \sqrt{p_1}\sigma_1$, $M_3 = \sqrt{p_3}\sigma_2$, and $M_4 = \sqrt{p_3}\sigma_3$ with $\sum_i p_i = 1$. The transformation of a single-qubit state under the Pauli channel is

$$\rho \mapsto p_0\rho + p_1\sigma_1\rho\sigma_1 + p_2\sigma_2\rho\sigma_2 + p_3\sigma_3\rho\sigma_3. \tag{9}$$

The experimental realization of the single-qubit Pauli channel is illustrated in Fig. 1(a), consisting of a sequence of LCs on the path of the second photon, one having its fast axis horizontal and the other oriented at 45° with respect to the horizontal [45,46]. Depending on the applied voltage V, it is possible to change the retardation between ordinary and extraordinary polarized radiations. That is, by applying either V_I or V_H to an LC in Fig. 1(b), it can be made to act as either a full wave or an HWP, respectively. Thus, by varying independently the voltages applied to LCs for different time intervals, we then apply the four Pauli operators to the second photon with different

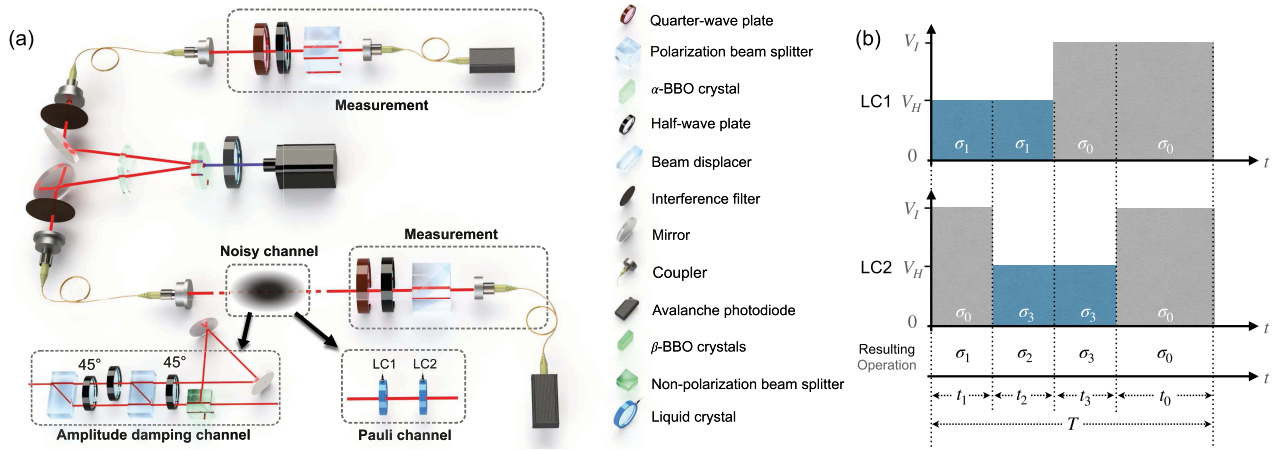

Fig. 1. Experimental setup. (a) Optical structure for the experiments. The entangled photon pairs are produced via the type-I spontaneous parametric down-conversion (SPDC) process by pumping two adjacent nonlinear crystals of BBO with a 405-nm laser diode. Two α-BBO crystals are inserted after the BBOs to compensate the walk-off effect. Mixed states emerge from the single-qubit noisy channel, such as the amplitude damping channel, the Pauli channel, the dephasing channel, and the depolarizing channel, acting on one of the qubits. Local measurements in $\mathcal{M}$ are carried out via a sequence of quarter-wave plate (QWP)-HWP-PBS and single-photon detection. Coincidence measurements are then performed via avalanche photodiodes (APDs). Total coincidence counts are about 120,000 over a collection time of 12 s within a 3-ns time window. (b) Schematic of the Pauli channel realized with two liquid crystals (LCs). Voltage sequences applied on the spatial path of photons. t_i indicates the time interval of voltage to realize the gate σ_i. T is the collection time. V_H is the corresponding applied voltage when an LC acts as an HWP, and V_I is for an identity operator.

values of the weight p. More precisely, the optical axes of LC_1 and LC_2 are fixed to 45° and 0° corresponding to the horizontal direction, respectively. Then, LC_1 and LC_2 act as an HWP at 45° (σ_1) and an HWP at 0° (σ_3), respectively, when voltage V_H is applied, whereas both LC_1 and LC_2 act as an identity operation (σ_0) when voltage V_I is applied. When both of the LCs are applied with V_H, the unit realizes a σ_2 operation. The weighted parameter p_i ($i \in \{0,1,2,3\}$) can be varied by changing the time-interval t_i, which corresponds to each σ_i of the voltage. By fixing the relative value of the probability parameters to $\{p_0, p_1, p_2, p_3\} = \{1 - p/6, p/12, p/18, p/36\}$, the number of parameters is reduced from 4 to 1. By setting the time intervals along with the relation $t_0 : t_1 : t_2 : t_3 = (1 - p/6) : p/12 : p/18 : p/36$, the Pauli channels with different values of parameter p are implemented. Here, $\sum_i t_i = T$, and T is the collection time.

To verify the validity of the method for experimental witnessing for entangled states with limited local measurements, we compare the witness values and the logarithmic negativity of the states [47,48]. The logarithmic negativity $E_{\mathcal{N}}(\rho) = \log_2 \|\rho^{\Gamma_B}\|_1$ is a notion of entanglement measure. Here, $\|\cdots\|_1$ denotes the trace norm, and Γ_B denotes the partial transpose. It varies between 0 and 1, indicating the separated and maximally entangled states, respectively, and can be evaluated with the states reconstructed via a full state tomography.

In the following, we show explicitly the performance of the witnesses on a family of pure states $|\phi\rangle$ [Eq. (7)] and mixed states [Eq. (8)], which emerge from several single-qubit quantum noisy channels.

In Fig. 2, we show the experimental results of the witness and negativity for both pure and mixed states. For pure states, the experimental results of $E_{\mathcal{N}}$ is 0 only when $\alpha = 0$, 1, which indicates the states are separated. As expected, for $\alpha = 0$ and 1, the experimental results of the entanglement witnesses are 0.0109 ± 0.0018 and 0.0093 ± 0.0017, respectively. For the rest states, $\mathrm{Tr}(W\rho)$ are always less than 0, which proves the method is effective in detecting entangled two-qubit pure states.

For the mixed states, which emerge from the Pauli channel, negativities are always larger than 0 (from 0.4812 ± 0.0049 to 0.3136 ± 0.0105) for $0 \le p \le 1$. As expected, the experimental results of the entanglement witnesses are less than 0 (from -0.4818 ± 0.0065 to -0.3194 ± 0.0059). Entanglement is detected for $0 \le p \le 1$. For the dephasing channel, the experimental results of the negativities decrease from 0.4505 ± 0.0060 to 0.0015 ± 0.0058 (the theoretical prediction is 0 for $p = 0.5$) and, then, increase to 0.4583 ± 0.0070. The experimental results of the entanglement witness increase from -0.4691 ± 0.0064 to 0.0152 ± 0.0055 for $0 \le p \le 0.5$ and decrease to -0.4748 ± 0.0064 for $0.5 < p \le 1$. For the depolarizing channel with $0 \le p < 0.5$, the experimental results of the negativity and the entanglement witness decrease from 0.4666 ± 0.0019 to 0 and increase from -0.4958 ± 0.0066 to 0.0182 ± 0.0052, respectively. For $p \ge 0.5$, the negativity is theoretically predicted to be 0, and the experimental results of the witness are larger than 0. This indicates the entanglement is detected for $0 \le p < 0.5$, and no entanglement is detected for $p \ge 0.5$. For the amplitude damping channel, the experimental results of the negativity are always larger than 0 for $0 \le p \le 1$. The experimental results of the entanglement witness are always less than 0. Entanglement is detected for $0 \le p \le 1$. Thus, the method of the construction and optimization of entanglement witnesses is valid for the family of the mixed states emerging from the noisy channels.

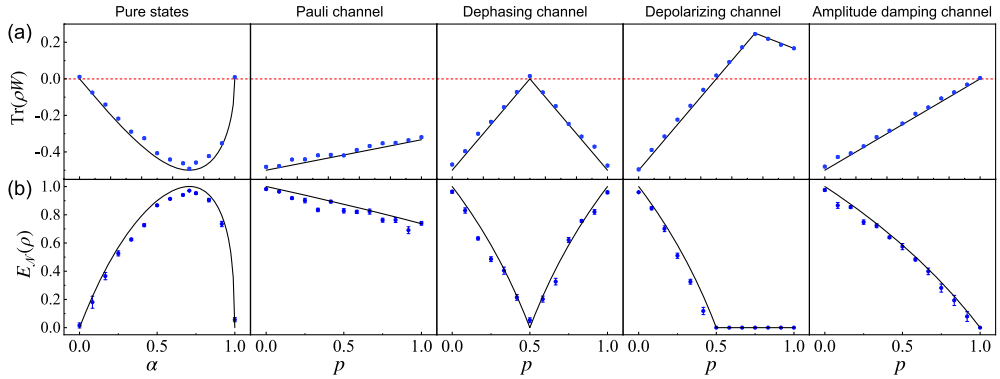

Fig. 2. Experimental results for two-qubit systems. (a) Entanglement witness value as a function of state parameter α for the pure states and of parameter p of the quantum noisy channels for the mixed states. (b) Negativities versus state parameter α or noisy parameter p. The solid curves indicate the theoretical predictions, and the symbols are for the experimental results. Error bar indicates the statistical uncertainty which is obtained via the Monte Carlo simulation method.

4. EXTENSIONS OF ENTANGLEMENT WITNESS TO HIGHER-DIMENSIONAL BIPARTITE SYSTEMS

Finally, we show the demonstration of extensions of entanglement witness to photonic higher-dimensional bipartite states [49–51], which are constructed with the limited local measurements. A straightforward generalization consists of the following:

$$W_{ijk} = |\varphi_i\rangle_{jk}\langle\varphi_i|^{\Gamma}_{jk}, \tag{10}$$

where

$$\begin{aligned}
|\varphi_1\rangle_{jk} &= a|\phi^+\rangle_{jk} + b|\phi^-\rangle_{jk},\\
|\varphi_2\rangle_{jk} &= a|\psi^+\rangle_{jk} + b|\psi^-\rangle_{jk},\\
|\varphi_3\rangle_{jk} &= a|\phi^+\rangle_{jk} + b|\psi^+\rangle_{jk},\\
|\varphi_4\rangle_{jk} &= a|\phi^-\rangle_{jk} + b|\psi^-\rangle_{jk},\\
|\varphi_5\rangle_{jk} &= a|\phi^+\rangle_{jk} + ib|\psi^-\rangle_{jk},\\
|\varphi_6\rangle_{jk} &= a|\phi^-\rangle_{jk} + ib|\psi^+\rangle_{jk},
\end{aligned}$$

and $|\phi^{\pm}\rangle_{jk} = (|jj\rangle \pm |kk\rangle)/\sqrt{2}$ and $|\psi^{\pm}\rangle_{jk} = (|jk\rangle \pm |kj\rangle)/\sqrt{2}$ are four Bell states, $a, b \in \mathbb{R}$, and satisfy $a^2 + b^2 = 1$. Note that for $d = 3$, W_{ijk} reduces to a fixed matrix with no parameter to optimize.

Another possible construction is of the so-called diagonal-type entanglement witness [52],

$$W = D - dP^+_d, \tag{11}$$

where $D = \sum_{i,j=1}^{d} d_{ij}|i\rangle\langle i| \otimes |j\rangle\langle j|$ is a $d \times d$ diagonal matrix, and P_d is a d-dimensional projector corresponding to a maximally correlated state $|\varphi\rangle = \sum_i x_i|ii\rangle$, satisfying $dP^+_d = \mathbb{F}^{\Gamma}$. Here, $\mathbb{F}$ is a so-called flip (or swap) operator defined as follows $\mathbb{F}\psi \otimes \phi = \phi \otimes \psi$ and $\langle\psi \otimes \phi|\mathbb{F}|\psi \otimes \phi\rangle = |\langle\psi|\phi\rangle|^2$ [52].

We consider $d = 3$ and

$$\begin{aligned}
D_{[abc]} = \sum_{i=1}^{3} |i\rangle\langle i| \otimes [&(a+1)|i\rangle\langle i| + b|i+1\rangle\langle i+1|\\
&+ c|i+2\rangle\langle i+2|],
\end{aligned} \tag{12}$$

where we add mod2 and $a, b, c \geq 0$. Then, $W_{[abc]} = D_{[abc]} - 3P^+_3$ is an entanglement witness [53] iff: $a < 2$, $a + b + c \geq 2$, and if $a < 1$, then, additionally, $bc > (1 - a)^2$. It is worth mentioning that the class $W_{[abc]}$ contains indecomposable entanglement witnesses iff $b \neq c$, which can be used to detect bound entangled states.

In our experiment, a family of three-dimensional bipartite states is used to demonstrate the above entanglement witnesses,

$$|\phi\rangle = c_0|00\rangle + c_1|11\rangle + c_2|12\rangle + c_3|21\rangle + c_4|22\rangle, \tag{13}$$

where $c_0 = \cos 2\theta_1$, $c_1 = \sin 2\theta_1 \cos 2\theta_2 \cos 2\theta_3$, $c_2 = -\sin 2\theta_1 \cos 2\theta_2 \sin 2\theta_3$, $c_3 = -\sin 2\theta_1 \sin 2\theta_2 \cos 2\theta_3$,

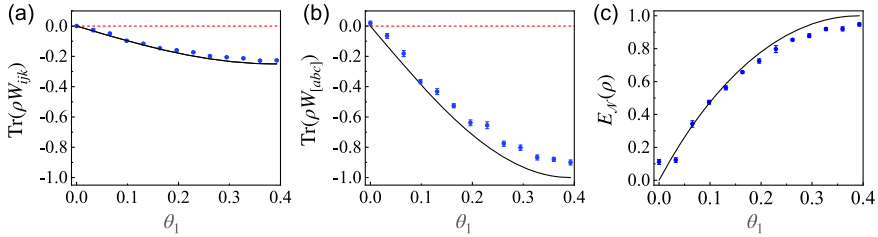

Fig. 3. Experimental results for higher-dimensional bipartite systems. (a) Values of the entanglement witness $\mathrm{Tr}(W_{ijk}\rho)$. (b) $\mathrm{Tr}(W_{[abc]}\rho)$ as functions of the parameter θ_1 of the states in Eq. (13). The solid curve indicates the theoretical predictions, and symbols are for the experimental results. (c) Logarithmic negativities of the states $E_N(\rho)$ versus the state parameter θ_1. Error bar indicates the statistical uncertainty which is obtained via the Monte Carlo simulation.

and $c_4 = \sin 2\theta_1 \sin 2\theta_2 \sin 2\theta_3$. We fix $\theta_2, \theta_3 = \pi/8$ and vary θ_1 from 0 to $\pi/8$ corresponding to the logarithmic negativity of the states varying from 0 to 1. Then, a similar optimization procedure is performed on the measurement results of $\mathcal{M}$ over the class of entanglement witnesses.

The experimental results of $\mathrm{Tr}(W_{ijk}\rho)$ and $\mathrm{Tr}(W_{[\mathrm{abc}]}\rho)$ are shown in Figs. 3(a) and 3(b), respectively. The negativities of the states in Fig. 3(c) increase from 0.1116 ± 0.0147 to 0.9477 ± 0.0095 with θ_1; the values of $\mathrm{Tr}(W_{ijk}\rho)$ and $\mathrm{Tr}(W_{[abc]}\rho)$ decrease from 0.0001 ± 0.0052 to -0.2262 ± 0.0041 and from 0.0190 ± 0.0134 to -0.9005 ± 0.0166, respectively. This indicates the validity of the proposed extensions of the entanglement witnesses to higher-dimensional bipartite systems.

5. CONCLUSION

We have reported an experimental demonstration of a method for construction of entanglement witnesses from a limited fixed set of local measurements ($\mathcal{M}$). The method required a classical optimization on the statistics of the results after performing the measurements within $\mathcal{M}$ and can be executed without knowing *a priori* information about the specific forms of the witnesses. Such a method is suitable for a scenario where only a limited local measurement resource (but not a full state tomography) is available. We tested the performance of the method on pure and mixed two-qubit entangled states, which were motivated by realistic experimental conditions, and we confirmed the method worked well for both cases, indicating that even a limited set of local measurements can be used for quick entanglement detection. Possible generalizations to higher-dimensional bipartite systems have been considered in our paper, whereas a similar analysis for the multipartite case still remains open to further study. The experimental accessibility of our method made it suitable for further development of other entanglement witnesses on higher-dimensional systems.

APPENDIX A: EXPERIMENTALLY REALIZING NOISY CHANNELS

The Kraus operators for a single-qubit dephasing channel are given by $M_1 = \sqrt{1-p}\sigma_0$ and $M_2 = \sqrt{p}\sigma_3$. The transformation of a single-qubit state under the dephasing channel is

$$\rho \to (1-p)\rho + p\sigma_3\rho\sigma_3. \tag{A1}$$

The Kraus operators for a single-qubit depolarizing channel are given by $M_1 = \sqrt{1-p}\sigma_0$, $M_2 = \sqrt{\frac{p}{3}}\sigma_1$, $M_3 = \sqrt{\frac{p}{3}}\sigma_2$, and $M_4 = \sqrt{\frac{p}{3}}\sigma_3$. Then, under the depolarizing channel, a single-qubit state evolves to

$$\rho \to (1-p)\rho + \frac{p}{3}(\sigma_1\rho\sigma_1 + \sigma_2\rho\sigma_2 + \sigma_3\rho\sigma_3). \tag{A2}$$

The dephasing channel and the depolarizing channel are actually two special cases of the Pauli channel. Their experimental realizations are similar to the Pauli channel in Fig. 1(a) of the main text.

For a single-qubit amplitude damping channel, the Kraus operators are given by $M_1 = |0\rangle\langle 0| + \sqrt{1-p}|1\rangle\langle 1|$ and $M_2 = \sqrt{p}|0\rangle\langle 1|$. The amplitude damping channel is experimentally realized by a dual interferometer setup [54–59] as shown in Fig. 1(a) of the main text. It is implemented by a Mach–Zehnder interferometer consisting of two beam displacers (BDs) and two HWPs at 45° and θ_p, respectively, followed by an HWP at 45°, a beam splitter (BS), and two mirrors. Photons with different polarizations are separated right after the interferometer and recombined at the BS. The optical path differently reduces the spatial coherence of the photons with different polarizations. By varying the setting angle of the HWP $\theta_p = \arcsin\sqrt{p}/2$, we are able to vary the parameter p of the amplitude damping channel.

APPENDIX B: IMPERFECTIONS IN OUR EXPERIMENT

The systematic shift between experimental results and theoretical predictions is caused by imperfection of state preparation, whereas the error bars are estimated through the statistical uncertainty of the photon numbers. Ideally, we prepare pure two-qubit entangled states and mixed two-qubit entangled states. Mixed entangled states emerge from four types of quantum noisy channels, i.e., Pauli channels, dephasing channels, depolarizing channels, and amplitude damping channels. However, in our experiment, the state preparation is not perfect, and the fidelity of the initial pure entangled state is about 97%, which is obtained by the state tomography.

In Fig. 4, we show the results of concurrence and negativity of the states emerging from a Pauli channel as an example to explain the systematic shift between experimental results and theoretical predictions. The blue line indicates the theoretical predictions obtained by the assumption of the perfect pure initial state,

$$|\Phi^+\rangle = \frac{1}{\sqrt{2}}(|00\rangle + |11\rangle), \tag{B1}$$

and the red line indicates the theoretical predictions obtained by the assumption of the mixed initial states. Without loss of generality, we assume the mixed initial states are Werner states,

$$\rho_w = \frac{4F-1}{3}|\Phi^+\rangle\langle\Phi^+| + \frac{1-F}{3}\mathbb{1}_4, \tag{B2}$$

where $F = \langle\Phi^+|\rho|\Phi^+\rangle = 97\%$ and $\mathbb{1}_4$ is a four-dimensional identity matrix. The symbols are for the experimental results. We can see that there is a shift between the lines, and the experimental results agree better with the theoretical predictions obtained by the assumption of the mixed initial states. Thus,

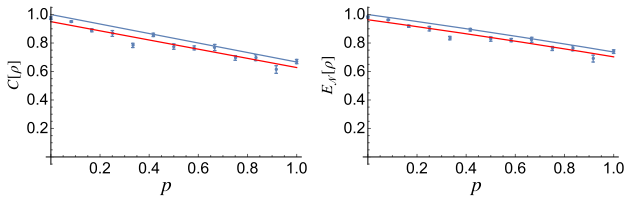

Fig. 4. Concurrence and negativity of the states versus the noisy parameter p of the Pauli channel. The blue line indicates the theoretical predictions obtained by the assumption of the perfect pure initial-state $|\Phi^+\rangle$, and the red line indicates the theoretical predictions obtained by the assumption of the mixed initial-state ρ_w. Symbols are for the experimental results. Error bar indicates the statistical uncertainty, which is obtained via the Monte Carlo simulation method.

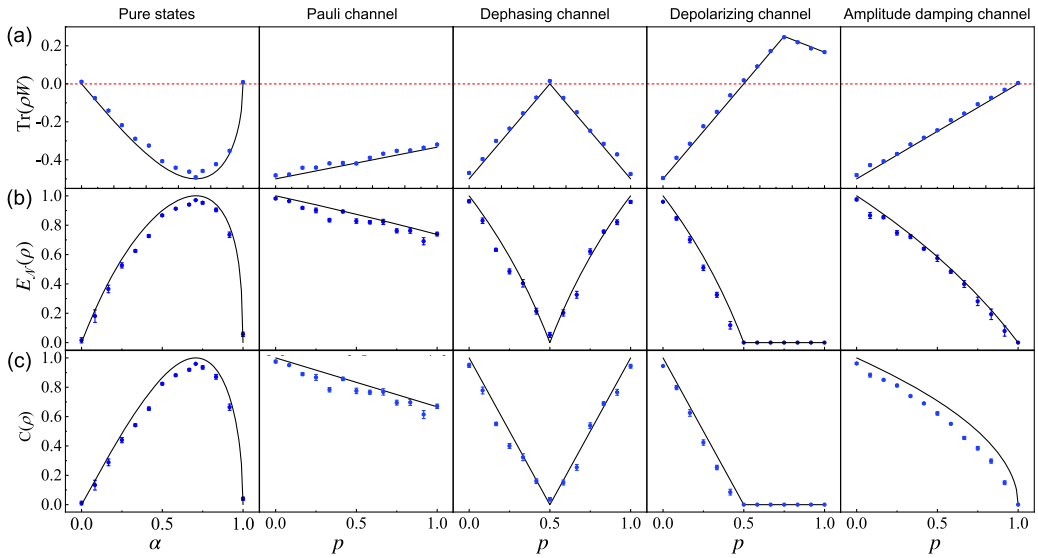

Fig. 5. (a) Entanglement witness value as a function of the state parameter α for the pure states and of parameter p of the quantum noisy channels for the mixed states. (b) Negativities and (c) concurrence versus state parameter α or noisy parameter p. The solid curves indicate the theoretical predictions, and the symbols are for the experimental results. Error bar indicates the statistical uncertainty, which is obtained via the Monte Carlo simulation method.

imperfection of the state preparation causes the systematic shift between the experimental results and their theoretical predictions as shown in Fig. 5 (the difference from Fig. 2 of the main text is that, here, we add the results of concurrence for entanglement measure).

APPENDIX C: HIGHER-DIMENSIONAL BIPARTITE SYSTEMS

Below, we discuss the possible generalizations to higher-dimensional bipartite systems. Similarly, the goal is to detect entanglement of bipartite qudit systems when only a limited fixed set of local measurements can be performed.

Any Hermitian operator in a d-dimensional system can be represented as

$$A = \sum_{j=0}^{d^2-1} c_j G_j, \tag{C1}$$

where $\{G_j\}$ is a set of local orthogonal observables (LOOs) in a d-dimensional system, which satisfies $\mathrm{Tr}(G_\alpha G_\beta) = \delta_{\alpha\beta}$, $(\alpha, \beta = 0, 1, \cdots, d^2)$. A convenient choice of such LOOs is generalized Gell–Mann matrices,

$$\begin{cases} G_l^D &= \sqrt{\frac{1}{l(l+1)}}\left(\sum_{j=1}^{l} |j\rangle\langle j| - l|l+1\rangle\langle l+1|\right), \\ & 1 \le l \le d-1; \\ G_{jk}^S &= (|j\rangle\langle k| + |k\rangle\langle j|)/\sqrt{2}, 1 \le j < k \le d; \\ G_{jk}^A &= (|j\rangle\langle k| - |k\rangle\langle j|)/i\sqrt{2}, 1 \le j < k \le d. \end{cases} \tag{C2}$$

Then, any Hermitian operator in a $d \times d$ system can be represented as

$$A = \frac{1}{d^2}\left[\mathbb{I}\otimes\mathbb{I} + \sum_{\alpha,\beta=1}^{d^2-1}(a_\alpha G_\alpha \otimes \mathbb{I} + b_\alpha \mathbb{I}\otimes G_\alpha) + \sum_{\alpha,\beta=1}^{d^2-1} C_{\alpha\beta} G_\alpha \otimes G_\beta\right], \tag{C3}$$

where a_α and b_α are real generalized Bloch vectors and $C_{\alpha\beta}$ is the correlation matrix. The canonical example of such a witness is provided by a flip operator $\mathbb{F} = \sum_{\alpha=0}^{d^2-1} G_\alpha \otimes G_\alpha$. As is well known, $\mathbb{F}$ witnesses entanglement within the whole class of $d \times d$ Werner states.

Similar to the scenario of qubit systems of Eq. (3) of the main text, here, we consider the class (we denote this class by $\mathcal{C}$) of entanglement witnesses of the form Eq. (C3) with the correlation matrix that satisfies the below structure,

$$\sum_{\alpha,\beta} C_{\alpha\beta} G_\alpha \otimes G_\beta = \sum_{k,l=1}^{d-1} D_{kl} G_k^D \otimes G_l^D + \sum_{i<j}(S_{ij} G_{ij}^S \otimes G_{ij}^S + A_{ij} G_{ij}^A \otimes G_{ij}^A). \tag{C4}$$

Thus, the analog (we denote it by $\mathcal{M}_d$) of the set of measurements $\mathcal{M}$ can be obtained accordingly. For the case of $d = 3$, the set is given by

$$\begin{aligned} \mathcal{M}_3 = \{&G_1^D \otimes G_1^D, G_2^D \otimes G_2^D, G_1^D \otimes G_2^D, G_2^D \otimes G_1^D; \\ &G_1^S \otimes G_1^S, G_2^S \otimes G_2^S, G_3^S \otimes G_3^S; \\ &G_1^A \otimes G_1^A, G_2^A \otimes G_2^A, G_3^A \otimes G_3^A\}. \end{aligned} \tag{C5}$$

As a straightforward generalization of the projections in Eq. (4) of the main text, it is proven in Ref. [42] that there are six families of rank-1 projectors $|\psi\rangle\langle\psi|$ within the class of Eq. (C4),

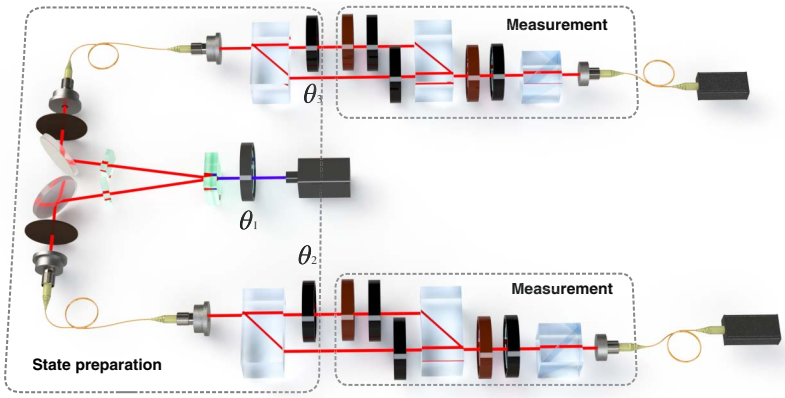

Fig. 6. Experimental setup for two-qutrit systems. The two-qutrit states are generated in the state preparation module, consisting of a set of SPDC entangled photon sources, two BDs, and two HWPs by employing the spatial and polarization modes of the photons. The local measurements and the state tomographic measurements are executed by the measurement modules, consisting of a sequence of HWPs, QWPs, a BD, and a PBS.

$$
\begin{aligned}
|\varphi_1\rangle_{jk} &= a|\Phi^+\rangle_{jk} + b|\Phi^-\rangle_{jk};\\
|\varphi_2\rangle_{jk} &= a|\Psi^+\rangle_{jk} + b|\Psi^-\rangle_{jk};\\
|\varphi_3\rangle_{jk} &= a|\Phi^+\rangle_{jk} + b|\Psi^+\rangle_{jk};\\
|\varphi_4\rangle_{jk} &= a|\Phi^-\rangle_{jk} + b|\Psi^-\rangle_{jk};\\
|\varphi_5\rangle_{jk} &= a|\Phi^+\rangle_{jk} + ib|\Psi^-\rangle_{jk};\\
|\varphi_6\rangle_{jk} &= a|\Phi^-\rangle_{jk} + ib|\Psi^+\rangle_{jk},
\end{aligned}
\tag{C6}
$$

where $|\Phi^{\pm}\rangle_{jk} = (|jj\rangle \pm |kk\rangle)/\sqrt{2}$ and $|\Psi^{\pm}\rangle_{jk} = (|jk\rangle \pm |kj\rangle)/\sqrt{2}$ are four Bell states; $a, b \in \mathbb{R}$ and satisfy $a^2 + b^2 = 1$.

One has, therefore, the analog of Eq. (5) of the main text for higher-dimensional bipartite systems,

$$
W_{ijk} = |\varphi_i\rangle_{jk}\langle\varphi_i|^{\Gamma}_{jk}, \tag{C7}
$$

with $i = 1, 2, \cdots, 6$.

Another possible construction is of the so-called diagonal-type entanglement witness [52],

$$
W = D - dP_d^+, \tag{C8}
$$

where $D = \sum_{i,j=1}^{d} d_{ij}|i\rangle\langle i| \otimes |j\rangle\langle j|$ is a $d \times d$ diagonal matrix and P_d is a d-dimensional projector corresponding to a maximally correlated state $|\varphi\rangle = \sum_i x_i|ii\rangle$, satisfying $dP_d^+ = \mathbb{F}^{\Gamma}$.

We consider $d = 3$ and

$$
\begin{aligned}
D_{[abc]} = \sum_{i=1}^{3} &|i\rangle\langle i| \otimes [(a+1)|i\rangle\langle i| + b|i+1\rangle\langle i+1|\\
&+ c|i+2\rangle\langle i+2|],
\end{aligned}
\tag{C9}
$$

where $a, b, c \geq 0$. An entanglement witness [53] $W_{[abc]} = D - dP_d^+$ is defined, iff $a < 2$, $a + b + c \geq 2$, and if $a < 1$, then, additionally $bc > (1-a)^2$, which can be used to detect bound entangled states.

The procedure for detection of the entanglement for a given bipartite qudit system is similar to that of a two-qubit system introduced earlier in this paper. For experimental demonstration, we consider the situation of $d = 3$, that is, entangled two-qutrit states, which are prepared by employing the spatial and polarization modes of the photons. Specifically, the bases $|0\rangle, |1\rangle, |2\rangle$ are encoded by the horizontal polarization of the photon in the lower mode and the vertical polarization and the horizontal polarization in the upper mode, respectively. The corresponding state preparation setup is shown in Fig. 6, consisting of a set of SPDC entangled photon sources, two BDs, and two HWPs. Then, the states are initialized to

$$
|\phi\rangle_{\theta} = c_1|00\rangle + c_2|11\rangle + c_3|12\rangle + c_4|21\rangle + c_5|22\rangle, \tag{C10}
$$

where $c_1 = \cos 2\theta_1$, $c_2 = \sin 2\theta_1 \cos 2\theta_2 \cos 2\theta_3$, $c_3 = -\sin 2\theta_1 \cos 2\theta_2 \sin 2\theta_3$, $c_4 = -\sin 2\theta_1 \sin 2\theta_2 \cos 2\theta_3$, and $c_5 = \sin 2\theta_1 \sin 2\theta_2 \sin 2\theta_3$. θ_1, θ_2, θ_3 are the angles of the corresponding HWPs in Fig. 6. In our experiment, θ_2 and θ_3 are fixed to $\pi/8$, and θ_1 varies from 0 to $\pi/8$, whereas the logarithmic negativity of the state changes from 0 to 1. The local measurements within $\mathcal{M}_3$ and the tomographic measurements are executed by two measurement modules, which consist of a sequence of HWPs and QWPs, a BD, and a PBS as illustrated in Fig. 6. Then, a similar optimization procedure is performed on the measurement results of $\mathcal{M}_3$ over the classes of entanglement witnesses proposed above for $d = 3$, that is, the decomposable entanglement witness W_{ijk} and the diagonal-type one $W_{[abc]}$. The results indicate the validity of the proposed extensions of the entanglement witnesses to higher-dimensional bipartite systems.

Funding. National Natural Science Foundation of China (12025401, U1930402, 12088101, 12104009, 12104036, 11734015).

Acknowledgment. G. Z. performed the experiments with contributions from C. Z., K. W., and L. X.; P. X. designed the experiments, analyzed the results, and wrote the paper.

Disclosures. The authors declare no conflicts of interest.

Data Availability. Data underlying the results presented in this paper are not publicly available at this time but may be obtained from the authors upon reasonable request.

REFERENCES

1. P. Xue and Y.-F. Xiao, "Universal quantum computation in decoherence-free subspace with neutral atoms," Phys. Rev. Lett. **97**, 140501 (2006).
2. Z. Bian, J. Li, H. Qin, X. Zhan, R. Zhang, B. C. Sanders, and P. Xue, "Realization of single-qubit positive-operator-valued measurement via a one-dimensional photonic quantum walk," Phys. Rev. Lett. **114**, 203602 (2015).
3. R. F. Werner, "Quantum states with Einstein-Podolsky-Rosen correlations admitting a hidden-variable model," Phys. Rev. A **40**, 4277–4281 (1989).
4. A. Peres, "Separability criterion for density matrices," Phys. Rev. Lett. **77**, 1413–1415 (1996).
5. O. Rudolph, "On the cross norm criterion for separability," J. Phys. A **36**, 5825 (2003).
6. K. Chen and L.-A. Wu, "A matrix realignment method for recognizing entanglement," arXiv:quant-ph/0205017 (2002).
7. P. Wocjan and M. Horodecki, "Characterization of combinatorially independent permutation separability criteria," Open Syst. Inf. Dyn. **12**, 331–345 (2005).
8. M. Horodecki, P. Horodecki, and R. Horodecki, "Separability of mixed quantum states: linear contractions and permutation criteria," Open Syst. Inf. Dyn. **13**, 103–111 (2006).
9. M. Horodecki, P. Horodecki, and R. Horodecki, "Separability of mixed states: necessary and sufficient conditions," Phys. Lett. A **223**, 1–8 (1996).
10. B. M. Terhal, "Bell inequalities and the separability criterion," Phys. Lett. A **271**, 319–326 (2000).
11. B. M. Terhal, "A family of indecomposable positive linear maps based on entangled quantum states," Linear Algebra Appl. **323**, 61–73 (2001).
12. B. M. Terhal, "Detecting quantum entanglement," Theor. Comput. Sci. **287**, 313–335 (2002).
13. G. Tóth and O. Gühne, "Detecting genuine multipartite entanglement with two local measurements," Phys. Rev. Lett. **94**, 060501 (2005).
14. F. A. Bovino, G. Castagnoli, A. Ekert, P. Horodecki, C. M. Alves, and A. V. Sergienko, "Direct measurement of nonlinear properties of bipartite quantum states," Phys. Rev. Lett. **95**, 240407 (2005).
15. O. Gühne and N. Lütkenhaus, "Nonlinear entanglement witnesses," Phys. Rev. Lett. **96**, 170502 (2006).
16. R. Augusiak, M. Demianowicz, and P. Horodecki, "Universal observable detecting all two-qubit entanglement and determinant-based separability tests," Phys. Rev. A **77**, 030301 (2008).
17. O. Gühne and G. Tóth, "Entanglement detection," Phys. Rep. **474**, 1–75 (2009).
18. O. Gühne, P. Hyllus, D. Bruß, A. Ekert, M. Lewenstein, C. Macchiavello, and A. Sanpera, "Detection of entanglement with few local measurements," Phys. Rev. A **66**, 062305 (2002).
19. O. Gühne and P. Hyllus, "Investigating three qubit entanglement with local measurements," Int. J. Theor. Phys. **42**, 1001–1013 (2003).
20. O. Gühne, P. Hyllus, D. Bruss, A. Ekert, M. Lewenstein, C. Macchiavello, and A. Sanpera, "Experimental detection of entanglement via witness operators and local measurements," J. Mod. Opt. **50**, 1079–1102 (2003).
21. C.-J. Zhang, Y.-S. Zhang, S. Zhang, and G.-C. Guo, "Optimal entanglement witnesses based on local orthogonal observables," Phys. Rev. A **76**, 012334 (2007).
22. B. Jungnitsch, T. Moroder, and O. Gühne, "Taming multiparticle entanglement," Phys. Rev. Lett. **106**, 190502 (2011).
23. M. Mozrzymas, A. Rutkowski, and M. Studziński, "Using non-positive maps to characterize entanglement witnesses," J. Phys. A: Math. Theor. **48**, 395302 (2015).
24. F. Shahandeh, M. Ringbauer, J. C. Loredo, and T. C. Ralph, "Ultrafine entanglement witnessing," Phys. Rev. Lett. **118**, 110502 (2017).
25. M. Gachechiladze, N. Wyderka, and O. Gühne, "The structure of ultrafine entanglement witnesses," J. Phys. A: Math. Theor. **51**, 365307 (2018).
26. S. Gerke, W. Vogel, and J. Sperling, "Numerical construction of multipartite entanglement witnesses," Phys. Rev. X **8**, 031047 (2018).
27. D. Chruściński, G. Sarbicki, and F. Wudarski, "Entanglement witnesses from mutually unbiased bases," Phys. Rev. A **97**, 032318 (2018).
28. S.-Q. Shen, T.-R. Xu, S.-M. Fei, X. Li-Jost, and M. Li, "Optimization of ultrafine entanglement witnesses," Phys. Rev. A **97**, 032343 (2018).
29. T. Simnacher, N. Wyderka, R. Schwonnek, and O. Gühne, "Entanglement detection with scrambled data," Phys. Rev. A **99**, 062339 (2019).
30. J. Bae, D. Chruściński, and B. C. Hiesmayr, "Mirrored entanglement witnesses," npj Quantum Inf. **6**, 15 (2020).
31. S.-Q. Shen, J.-M. Liang, M. Li, J. Yu, and S.-M. Fei, "Nonlinear improvement of qubit-qudit entanglement witnesses," Phys. Rev. A **101**, 012312 (2020).
32. T. Li, L.-M. Lai, D.-F. Liang, S.-M. Fei, and Z.-X. Wang, "Entanglement witnesses based on symmetric informationally complete measurements," Int. J. Theor. Phys. **59**, 3549–3557 (2020).
33. M. Barbieri, F. De Martini, G. Di Nepi, P. Mataloni, G. M. D'Ariano, and C. Macchiavello, "Detection of entanglement with polarized photons: experimental realization of an entanglement witness," Phys. Rev. Lett. **91**, 227901 (2003).
34. G. Lima, E. S. Gómez, A. Vargas, R. O. Vianna, and C. Saavedra, "Fast entanglement detection for unknown states of two spatial qutrits," Phys. Rev. A **82**, 012302 (2010).
35. J. Dai, Y. L. Len, Y. S. Teo, B.-G. Englert, and L. A. Krivitsky, "Experimental detection of entanglement with optimal-witness families," Phys. Rev. Lett. **113**, 170402 (2014).
36. F. Brange, O. Malkoc, and P. Samuelsson, "Minimal entanglement witness from electrical current correlations," Phys. Rev. Lett. **118**, 036804 (2017).
37. N. Friis, G. Vitagliano, M. Malik, and M. Huber, "Entanglement certification from theory to experiment," Nat. Rev. Phys. **1**, 72–87 (2019).
38. B. Dirkse, M. Pompili, R. Hanson, M. Walter, and S. Wehner, "Witnessing entanglement in experiments with correlated noise," Quantum Sci. Technol. **5**, 035007 (2020).
39. G. Zhu, D. Dilley, K. Wang, L. Xiao, E. Chitambar, and P. Xue, "Less entanglement exhibiting more nonlocality with noisy measurements," npj Quantum Inf. **7**, 166 (2021).
40. R. Horodecki, P. Horodecki, M. Horodecki, and K. Horodecki, "Quantum entanglement," Rev. Mod. Phys. **81**, 865–942 (2009).
41. M. Lewenstein, B. Kraus, J. I. Cirac, and P. Horodecki, "Optimization of entanglement witnesses," Phys. Rev. A **62**, 052310 (2000).
42. A. Riccardi, D. Chruściński, and C. Macchiavello, "Optimal entanglement witnesses from limited local measurements," Phys. Rev. A **101**, 062319 (2020).
43. R. Jozsa, "Fidelity for mixed quantum states," J. Mod. Opt. **41**, 2315–2323 (1994).
44. J. Fiurášek, "Maximum-likelihood estimation of quantum measurement," Phys. Rev. A **64**, 024102 (2001).
45. A. Chiuri, V. Rosati, G. Vallone, S. Pádua, H. Imai, S. Giacomini, C. Macchiavello, and P. Mataloni, "Experimental realization of optimal noise estimation for a general Pauli channel," Phys. Rev. Lett. **107**, 253602 (2011).
46. A. Orieux, L. Sansoni, M. Persechino, P. Mataloni, M. Rossi, and C. Macchiavello, "Experimental detection of quantum channels," Phys. Rev. Lett. **111**, 220501 (2013).
47. K. Życzkowski, P. Horodecki, A. Sanpera, and M. Lewenstein, "Volume of the set of separable states," Phys. Rev. A **58**, 883–892 (1998).
48. G. Vidal and R. F. Werner, "Computable measure of entanglement," Phys. Rev. A **65**, 032314 (2002).
49. G. Zhu, O. Kálmán, K. Wang, L. Xiao, D. Qu, X. Zhan, Z. Bian, T. Kiss, and P. Xue, "Experimental orthogonalization of highly overlapping quantum states with single photons," Phys. Rev. A **100**, 052307 (2019).
50. Z. Bian, L. Xiao, K. Wang, F. A. Onanga, F. Ruzicka, W. Yi, Y. N. Joglekar, and P. Xue, "Quantum information dynamics in a high-dimensional parity-time-symmetric system," Phys. Rev. A **102**, 030201 (2020).

51. X. Zhan, X. Zhang, J. Li, Y. Zhang, B. C. Sanders, and P. Xue, "Realization of the contextuality-nonlocality tradeoff with a qubit-qutrit photon pair," Phys. Rev. Lett. **116**, 090401 (2016).
52. D. Chruściński and G. Sarbicki, "Entanglement witnesses: construction, analysis and classification," J. Phys. A **47**, 483001 (2014).
53. K.-C. Ha, "Atomic positive linear maps in matrix algebras," Publ. Res. Inst. Math. Sci. **34**, 591–599 (1998).
54. L. Xiao, T. Deng, K. Wang, G. Zhu, Z. Wang, W. Yi, and P. Xue, "Non-Hermitian bulk–boundary correspondence in quantum dynamics," Nat. Phys. **16**, 761–766 (2020).
55. L. Xiao, K. Wang, X. Zhan, Z. Bian, K. Kawabata, M. Ueda, W. Yi, and P. Xue, "Observation of critical phenomena in parity-time-symmetric quantum dynamics," Phys. Rev. Lett. **123**, 230401 (2019).
56. P. Xue, R. Zhang, H. Qin, X. Zhan, Z. H. Bian, J. Li, and B. C. Sanders, "Experimental quantum-walk revival with a time-dependent coin," Phys. Rev. Lett. **114**, 140502 (2015).
57. K. K. Wang, X. Qiu, L. Xiao, X. Zhan, Z. Bian, B. C. Sanders, W. Yi, and P. Xue, "Observation of emergent momentum-time skyrmions in parity-time-symmetric non-unitary quench dynamics," Nat. Commun. **10**, 2293 (2019).
58. L. Xiao, X. Zhan, Z. Bian, K. Wang, X. Wang, J. Li, K. Mochizuki, D. Kim, N. Kawakami, W. Yi, H. Obuse, B. C. Sanders, and P. Xue, "Observation of topological edge states in parity-time-symmetric quantum walks," Nat. Phys. **13**, 1117–1123 (2017).
59. K. Wang, X. Qiu, L. Xiao, X. Zhan, Z. Bian, W. Yi, and P. Xue, "Simulating dynamic quantum phase transitions in photonic quantum walks," Phys. Rev. Lett. **122**, 020501 (2019).